AIAA SciTech Forum
11–15 & 19–21 January 2021, VIRTUAL EVENT
AIAA Scitech 2021 Forum

10.2514/6.2021-1387

Design and Control of a Tensegrity Torus Spacecraft Composed of Reconfigurable Units

Alexander M. Popescu*, Raman Goyal†, and Manoranjan Majji‡
Texas A&M University, College Station, Texas, 77843, USA

Design details of a modular torus composed of a network of axially loaded members are discussed in this paper. Each module is shown to be a tensegrity system, that makes an optimal use of mass to take the loads imposed on the structural system. The use of optimal compressive structures enables the design to offer resistance to the tangential hoop stresses caused due to centrifugal forces. While the dual T-bar design is used to minimize the support mass for space applications, the current topological considerations are shown to accommodate a combination of T and D-bar topologies for the construction of the torus. Embedded wheels in the design are shown to maximize the inertia of the torus per unit mass. Principles of Eulerian mechanics are utilized to control the torus with embedded reaction wheels. Lyapunov stability theory is used to derive stable nonlinear control laws to control the attitude of the torus.

I. Nomenclature

N	=	number of modules
n	=	number of reaction wheels
R_o	=	torus major radius
ℓ	=	plate edge length
$\hat{\mathbf{a}}_i$	=	spin direction of the i^{th} reaction wheel
J_{si}	=	i^{th} reaction wheel moment of inertia in spin direction
J_{ti}	=	i^{th} reaction wheel moment of inertia transverse to spin direction
$\mathbf{r}_{ji}$	=	position of the jth reaction wheel of module i
$\mathbf{q}$	=	quaternion attitude vector representation
$\mathbf{q}_d$	=	reference attitude quaternion
$\boldsymbol{\omega}$	=	spacecraft angular velocity

II. Introduction

Tensegrity structures are stable networks of axially loaded members [1, 2]. These members are either in tension (cables), or in compression (bars). Tensegrity structures are divided into two categories: class-1 structures, where no bars are connected to each other, and class-k structures, where k bars are connected through ball joints [3]. The connection through ball joints allows for the overall system to bend without creating any bending moment/torque on any individual member of the structure [4, 5]. The absence of bending moments indicates that the deforming force in each member is only in one direction, which leads to reliable high-precision mathematical models and forms the basis to develop optimum mass structures [6, 7].

Tensegrity T-bar and D-bar structures have been analytically shown to support compressive loads with minimum mass compared to continuum compressive columns [3]. Tensegrity structures have further been shown to provide minimum mass designs to take simply supported and cantilever loading condition [8, 9]. The numerous equilibrium configurations achievable through prestressable strings allow the structure to demand minimal control energy to change its shape as the structure will move from one equilibrium configuration to another equilibrium configuration [10, 11]. All the above-mentioned properties have lead researchers to study tensegrity structures for different applications ranging from civil engineering [9, 12] to aerospace engineering [13, 14]. Different dynamics models have also been formulated

*Graduate Research Assistant, Aerospace Engineering, 3141-TAMU, and Student Member, AIAA
†TEES Postdoctoral Research Associate, Aerospace Engineering, 3141-TAMU, and Member, AIAA
‡Assistant Professor, Director, LASR Laboratory, Aerospace Engineering, Associate Fellow, AIAA

to cater to the needs of these applications using tensegrity structures [7, 15, 16]. By the addition of reaction wheels to a class of tensegrity systems, it was recently shown that gyroscopic torques may be imparted on the structural system. [17]. This new gyroscopic tensegrity system can be used to further enhance the multifunctional nature of tensegrity systems.

Momentum wheels (or reaction wheels) and control moment gyroscopes (CMGs) are used in the attitude control of spacecraft [18]. In large space structures such as the International Space Station (ISS), Hubble Space Telescope (HST), attitude control is accomplished by generating a large gyroscopic torque using massive wheels arranged on steerable gimbals [19, 20].

Space habitat designs with reaction wheels to control the attitude have also been proposed in the literature. An important aspect of space habitats is to create artificial gravity and multiple designs have been discussed in the past for the feasibility analysis of the habitat concepts. In 1952, Wernher Von Braun proposed a torus/wheel shaped space station (The Gateway Foundation), as a low earth orbit cruise ship to accommodate around 1500 people [21]. However, the design did not receive more detailed studies in the coming years due to difficult growth strategy and inefficient use of the habitat volume compared to the concentric cylinder concept [22]. However, the torus design can be used for relatively smaller space structures. A more fundamental question in space engineering is the development of modular space structures that can be composed into larger units like the habitat systems. It is of consequence to make the modular units to have power, attitude determination, control, sensing, communication and computations, so that a distributed set of space systems can be assembled to realize a multifunctional space system such as the space habitat.

This paper is focused on the design and control of a toroidal truss structure formed using reconfigurable tensegrity units. Traditional tensegrity modules are equipped with reaction wheels to impart gyroscopic actuation capabilities to the toroidal truss. The design is focused on the efficient arrangement of gyroscopic wheels for the attitude control of the tensegrity torus. This demonstrates the realization of a multifunctional modular structural design that can function as an autonomous space system. A systematic approach to optimize the distribution of large angular momentum generated using the massive monolithic wheel to smaller angular momentum generation using small reaction wheels at multiple locations is devised in the paper. Dynamics and control principles are utilized to demonstrate the efficacy of the modular toroidal structure by showcasing representative attitude control strategies using the momentum management of the network of wheels used in the design process. This demonstration forms the basis for in-space manufacturing and automated assembly of habitat systems.

The paper is organized as follows: Fundamental topological design details of the T-Bar module with embedded reaction wheels are discussed using the kinematics and kinetics of a single module. This is followed by the details of the assembly of individual modules to realize larger structural systems of a general topological chain. The technical details of an assembly that forms a torus structure are then demonstrated as an example. This is followed by the dynamical equations of motion for the assembly. Attitude control details are then presented, along with the details on control allocation of the commanded torque among the individual reaction wheel modules. Numerical simulations to illustrate the utility of the proposed design concepts are then described. Some important conclusions on the utility of the broad ideas of the proposed approach for in-space manufacturing applications conclude the paper.

III. T-Bar Module Design

A three-dimensional T-Bar is a basic class-5 tensegrity structure that is capable of supporting compressive loads applied at both of its endpoints [3]. Skelton *et al.* found that T-Bar structures with self-similar repetitions are able to reduce total mass compared to a single beam under identical compressive load, and subject to local buckling strength constraints on each bar [6]. Furthermore, an algorithm was also developed to consider the global buckling analysis of the T-bar tensegrity system along with the local yielding and buckling failures of each individual member. Thus, T-Bar tensegrities are favorable candidates for space structural applications as they can reduce spacecraft mass.

A gyroscopic T-Bar design is now presented, wherein a T-Bar structure is equipped with three reaction wheels (also known as gyroscopes) affixed to a central plate, as illustrated in fig. 1. The addition of these gyroscopes allows the attitude and angular velocity of each T-Bar unit to be controlled independently of any other units. Nonlinear dynamical models of tensegrity structures (including the T-Bar) with embedded gyroscopes have recently been formulated in [17]. While earlier designs associated with the gyroscopic tensegrity systems included the wheels on the compressive structures, this new T-Bar design moves the wheels to the plates for two distinct advantages. Firstly, this ensures the mass center of the module remains close to the geometric center of the T-Bar module. Secondly, and more importantly, since the wheels generate moments primarily along the perpendicular direction of their axis of rotation, the gyroscopic torques impose a bending moment on the bar, if they are placed or installed at the center of the bar, with the axis of symmetry of the wheel is collocated with the bar vector. By moving the wheel to the node location, the moments on the

compressive members are relieved, in keeping with the traditional objectives of tensegrity systems.

We note that in our design, the central plate is attached to two bars on either side through ball joints. There are six strings per module.

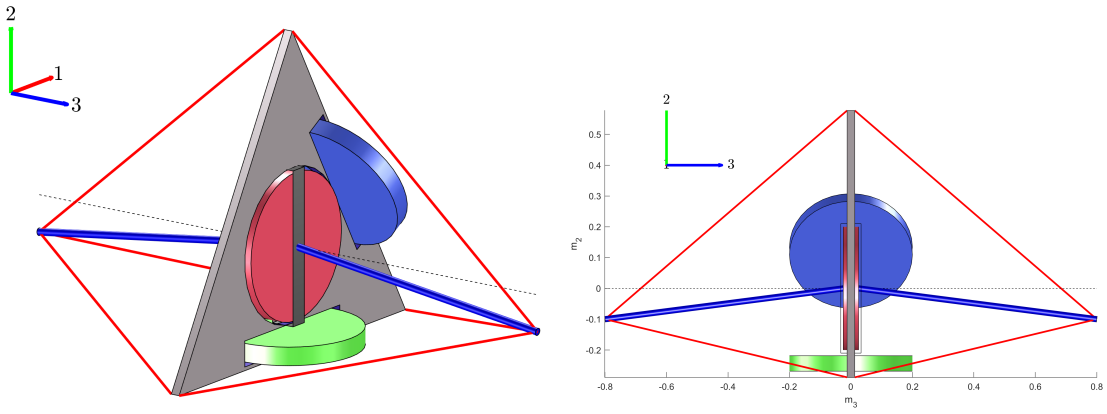

Fig. 1 (Left) Perspective view of proposed modular structural unit. (Right) Front view of modular unit. There are 2 bars (blue), 6 strings (red), a central plate structure (grey), and 3 reaction wheels (red, blue, green) attached to the central plate.

The wheels are labeled as follows: 1:red, 2:green, 3:blue. A dextral coordinate frame $M = \{\hat{\mathbf{m}}_1, \hat{\mathbf{m}}_2, \hat{\mathbf{m}}_3\}$ is defined for each module (shown in figure 1). The origin of M is at the center of the triangular plate and is concentric with reaction wheel 1. We can write the spin axis of each reaction wheel, which is denoted as $\hat{\mathbf{a}}_i$ as:

$$\hat{\mathbf{a}}_1 = \hat{\mathbf{m}}_3, \qquad \hat{\mathbf{a}}_2 = \hat{\mathbf{m}}_2, \qquad \hat{\mathbf{a}}_3 = \frac{\sqrt{3}}{2}\hat{\mathbf{m}}_1 + \frac{1}{2}\hat{\mathbf{m}}_2. \tag{1}$$

Note that the spin axis unit vectors $\{\hat{\mathbf{a}}_1, \hat{\mathbf{a}}_2, \hat{\mathbf{a}}_3\} \in \mathbb{R}^3$, which means that these wheels can achieve a net torque vector in any direction.

The position vectors for center of the wheels are located at:

$$\mathbf{r}_1 = \mathbf{0}, \qquad \mathbf{r}_2 = -h_{rw}\hat{\mathbf{m}}_2, \qquad \mathbf{r}_3 = h_{rw}\frac{\sqrt{3}}{2}\hat{\mathbf{m}}_1 + h_{rw}\frac{1}{2}\hat{\mathbf{m}}_2, \tag{2}$$

where h_{rw} is the distance from the origin of M to the center of wheels 2 and 3. The central plate is an equilateral triangle with edge length ℓ, where $h_{rw} < \ell/2\sqrt{3}$.

IV. Building a Larger Structure

Multiple aforementioned T-Bar building blocks can be assembled in series to form a larger overall space truss that has the ability to generate moments, in addition to bearing the requisite compressive loads necessary for a regular space truss. By controlling the reaction wheel speeds and the string lengths, we are able to reconfigure (reshape) the overall structure to achieve a wide range of serpentine-like shapes. Furthermore, the modules can be deployed in space and assembled to achieve a larger class of topological shapes and functions akin to other space truss structures used in space manufacturing. The modular nature of the proposed spacecraft also allows for in-space assembly and attachment of each unit. While the topological realizations of the passive and active (reconfigurable) arrangements of the T-Bar building blocks are innumerable, this paper focusses on a torus topology to demonstrate the key features of the gyroscopic tensegrity systems.

V. Torus Structure

Consider a torus structure which is built out of N T-Bar units, arranged end-to-end in a circle, as shown in fig. 2. We make a slight modification to the T-Bar unit by moving the string attachment points from the two bar endpoints, to the

center of the adjacent plates, so as to interleave the strings of adjacent units. In addition to the bars and strings of each unit, we also add strings between the vertices of each adjacent plate. This increases the rotational stability between units.

Because of the modular nature of the structure, we can swap T-Bar modules with other tensegrity units, such as a D-Bar [3], with minimal adjustments to other modules. To simplify our analysis, we assume that all strings will remain constant length, so that the entire torus behaves as a single rigid body.

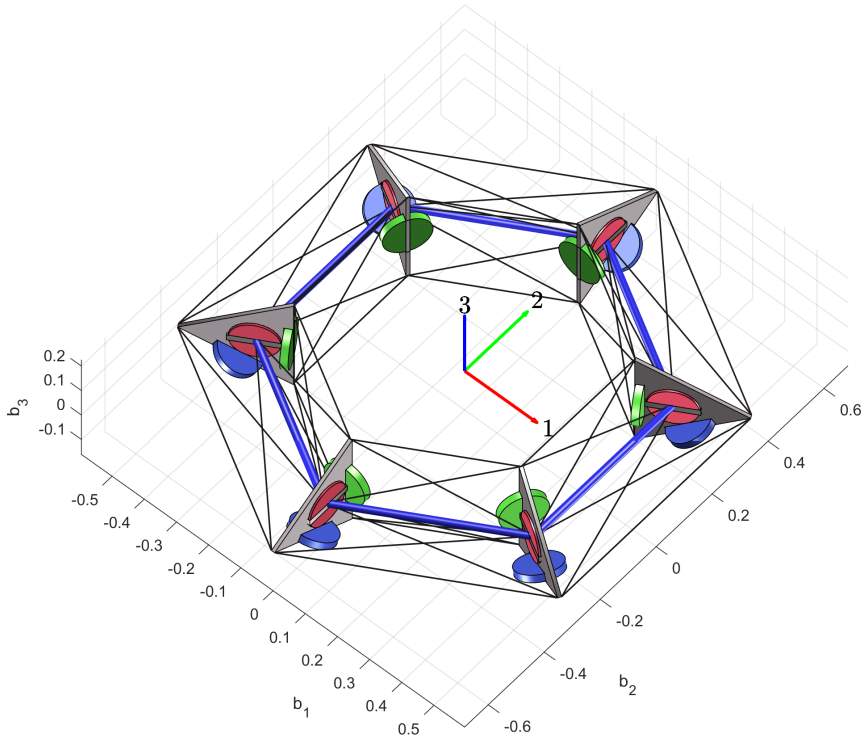

Fig. 2 Perspective view of assembled spacecraft composed of $N = 6$ T-Bar units. Bars are denoted by solid blue cylinders, while strings are represented by thin gray lines. The body frame basis vectors are depicted in the center.

We define the spacecraft body frame $B = \{\hat{\mathbf{b}}_1, \hat{\mathbf{b}}_2, \hat{\mathbf{b}}_3\}$ to be affixed to the rigid-body spacecraft. The origin of the B frame is chosen to be at the center of mass (COM) of the spacecraft. Let there be N T-Bar modules in the torus. We can find the basis vectors of the i^{th} module's coordinate frame M_i, $i = 0, 1, 2, \ldots, N-1$, with

$$\hat{\mathbf{m}}_{1i} = -\hat{\mathbf{b}}_3, \qquad \hat{\mathbf{m}}_{2i} = \sin(\varphi i)\hat{\mathbf{b}}_1 + \cos(\varphi i)\hat{\mathbf{b}}_2, \qquad \hat{\mathbf{m}}_{3i} = \cos(\varphi i)\hat{\mathbf{b}}_1 - \sin(\varphi i)\hat{\mathbf{b}}_2, \tag{3}$$

where $\varphi = 2\pi/N$ is the radial angle between adjacent modules and the origin of M_i is simply

$$\mathbf{O}_{M_i} = R_o\hat{\mathbf{m}}_{2i} - \mathbf{r}_{COM}, \tag{4}$$

where R_o is the major radius of the torus and $\mathbf{r}_{COM}$ is the COM position of the entire torus structure. The position of the j^{th} reaction wheel of module i, $\mathbf{r}_{ji}$, is

$$\mathbf{r}_{1i} = \mathbf{O}_{M_i}, \tag{5}$$

$$\mathbf{r}_{2i} = \mathbf{O}_{M_i} - \hat{\mathbf{m}}_{2i}h_{rw}, \tag{6}$$

$$\mathbf{r}_{3i} = \mathbf{O}_{M_i} + \hat{\mathbf{m}}_{1i}h_{rw}\frac{\sqrt{3}}{2} + \hat{\mathbf{m}}_{2i}h_{rw}\frac{1}{2}, \tag{7}$$

with $i = 0, 1, 2, \ldots N-1$. The spin axis of the j^{th} reaction wheel of module i, $\hat{\mathbf{a}}_{ji}$, is

$$\hat{\mathbf{a}}_{1i} = \hat{\mathbf{m}}_{3i}, \tag{8}$$

$$\hat{\mathbf{a}}_{2i} = \hat{\mathbf{m}}_{2i}, \tag{9}$$

$$\hat{\mathbf{a}}_{3i} = \hat{\mathbf{m}}_{1i}\frac{\sqrt{3}}{2} + \hat{\mathbf{m}}_{2i}\frac{1}{2}. \tag{10}$$

VI. Equations of Motion

To simplify our analysis, we assume that all strings will remain constant length, so that the entire torus behaves as a single rigid body. The equations of motion of a rigid-body spacecraft with n reaction wheels rigidly affixed to it are developed in this section. If $n > 3$ and the wheel spin axes are independent, the reaction wheels are said to form a redundant set. We base our analysis on [23, 24].

A. Equations of Motion of a Single Wheel

The inertia matrix of the i^{th} wheel about its center of mass is [20]

$$\mathbf{J}^B_{cwi} = J_{ti}\mathbf{I}_3 + (J_{si} - J_{ti})\hat{\mathbf{a}}_i\hat{\mathbf{a}}_i^T, \tag{11}$$

where $\hat{\mathbf{a}}_i$ is spin axis of i^{th} wheel, J_{si} is the inertia of i^{th} wheel about its symmetry axis, J_{ti} is the inertia of i^{th} wheel about any perpendicular axis, and $\mathbf{I}_3$ is the 3×3 identity matrix. The angular momentum of the i^{th} wheel about its COM can then be written as:

$$\mathbf{h}_{cwi} = J_{si}\omega_{si}\hat{\mathbf{a}}_i + \mathbf{J}^B_{cwi}\boldsymbol{\omega}_{B/N}, \tag{12}$$

where ω_{si} is the scalar angular speed of wheel i with respect to the body, and $\boldsymbol{\omega}_{B/N}$ is the angular velocity of the body with respect to an inertial frame N. The component of the wheel's angular momentum in the direction of its spin axis is

$$h_{ai} = J_{si}(\omega_{si} + \hat{\mathbf{a}}_i^T\boldsymbol{\omega}_{B/N}). \tag{13}$$

By utilizing Euler's Equation, we can solve for the net external torque applied in the wheel spin direction as:

$$L_{ai} = \hat{\mathbf{a}}_i^T\mathbf{L}_{cwi} = J_{si}(\dot{\omega}_{si} + \hat{\mathbf{a}}_i^T\dot{\boldsymbol{\omega}}_{B/N}). \tag{14}$$

We also note that

$$\dot{h}_{ai} = J_{si}(\dot{\omega}_{si} + (\boldsymbol{\omega}_{B/N} \times \hat{\mathbf{a}}_i)^T\boldsymbol{\omega}_{B/N} + \hat{\mathbf{a}}_i^T\dot{\boldsymbol{\omega}}_{B/N}) = L_{ai}, \tag{15}$$

where L_{ai} is the torque applied by the i^{th} motor actuator to the i^{th} wheel, and represents a control input to our system.

B. Body Frame Dynamics

We define the composite inertia matrix $\mathbf{J}^B_c$ which contains the inertia of the spacecraft and wheels plus only the transverse components of the wheel inertias as:

$$\mathbf{J}^B_c = \mathbf{J}^B_{c,\text{no wheels}} - \sum_{i=1}^{n} m_{wi}[\mathbf{b}_i\times]^2 + \sum_{i=1}^{n} J_{ti}(\mathbf{I}_3 - \hat{\mathbf{a}}_i\hat{\mathbf{a}}_i^T), \tag{16}$$

where $\mathbf{J}^B_{c,\text{no wheels}}$ is the inertia matrix of the spacecraft without any wheels, m_{wi} is the mass of wheel i, and $\mathbf{b}_i$ is the position of the COM of wheel i in the body frame. The parallel axis theorem was utilized to arrive at this expression [25]. The matrix $[\mathbf{b}_i\times]$ denotes the 3×3 cross product matrix formed from $\mathbf{b}_i$, defined by:

$$[\mathbf{a}\times] = \begin{bmatrix} 0 & -a_3 & a_2 \\ a_3 & 0 & -a_1 \\ -a_2 & a_1 & 0 \end{bmatrix}. \tag{17}$$

The total momentum of the spacecraft can be written using eqs. (13) and (16) as

$$\mathbf{h}_c = \mathbf{J}^B_c\omega_{B/N} + \sum_{i=1}^{n} h_{ai}\hat{\mathbf{a}}_i. \tag{18}$$

Finally, application of Euler's Equation yields the spacecraft equations of motion, which are also stated identically in [23]:

$$\mathbf{J}_c^B \dot{\boldsymbol{\omega}}_{B/N} = -\mathbf{G}\mathbf{u} - \boldsymbol{\omega}_{B/N} \times \left(\mathbf{J}_c^B \boldsymbol{\omega}_{B/N} + \mathbf{G}\mathbf{h}_a\right) + \mathbf{L}_c^B, \tag{19}$$

$$\dot{\mathbf{h}}_a = \mathbf{u}, \tag{20}$$

with

$$\mathbf{G} = \begin{bmatrix} \hat{\mathbf{a}}_1 & \hat{\mathbf{a}}_2 & \cdots & \hat{\mathbf{a}}_n \end{bmatrix}, \qquad \mathbf{u} = \begin{bmatrix} L_{a1} & L_{a2} & \cdots & L_{an} \end{bmatrix}^T, \tag{21}$$

$$\mathbf{h}_a = \begin{bmatrix} h_{a1} & h_{a2} & \cdots & h_{an} \end{bmatrix}^T, \tag{22}$$

where $\mathbf{u} \in \mathbb{R}^n$ is the control input to the system, and $\mathbf{L}_c^B$ is the net external torque. If we additionally choose a quaternion representation of attitude, we also have the quaternion dynamics equation [24] given as:

$$\dot{\mathbf{q}} = \frac{1}{2}\Omega(\boldsymbol{\omega})\mathbf{q}, \tag{23}$$

$$\Omega(\boldsymbol{\omega}) = \begin{bmatrix} -[\boldsymbol{\omega}\times] & \boldsymbol{\omega} \\ -\boldsymbol{\omega}^T & 0 \end{bmatrix}. \tag{24}$$

C. Energy and Power

The reaction wheels can add or subtract mechanical kinetic energy to the spacecraft system as they apply torque to spin the spacecraft. We now investigate the total mechanical kinetic energy of the spacecraft. The total kinetic energy of the system is given by [24]

$$T = \frac{1}{2}\boldsymbol{\omega}^T \mathbf{J}_c^B \boldsymbol{\omega} + \frac{1}{2}\sum_{i=1}^{n} J_{si}(\omega_{si} + \boldsymbol{\omega}^T \hat{\mathbf{a}}_i)^2, \tag{25}$$

$$= \frac{1}{2}\boldsymbol{\omega}^T \mathbf{J}_c^B \boldsymbol{\omega} + \frac{1}{2}\sum_{i=1}^{n} h_{ai}^2/J_{si}, \tag{26}$$

where $\boldsymbol{\omega}$ is the angular velocity of the body frame in an inertial frame. The mechanical power of the spacecraft is found by differentiating eq. (26):

$$\dot{T} = \boldsymbol{\omega}^T \mathbf{J}_c^B \dot{\boldsymbol{\omega}} + \mathbf{h}_a^T \mathbf{J}_s^{-1} \mathbf{u}, \tag{27}$$

where $\mathbf{J}_s = \text{diag}([J_{s1}, J_{s2}, \ldots, J_{sn}])$. We plug in eq. (19) with $\mathbf{L}_c^B = \mathbf{0}$ to obtain

$$\dot{T} = \sum_{i=1}^{n} \omega_{si} u_i = \mathbf{h}_a^T \mathbf{J}_s^{-1} \mathbf{u} - \boldsymbol{\omega}^T \mathbf{G}\mathbf{u} = (\mathbf{h}_a^T \mathbf{J}_s^{-1} - \boldsymbol{\omega}^T \mathbf{G})\mathbf{u}. \tag{28}$$

VII. Attitude Control

A. Attitude Regulation

Several feedback attitude controllers are described in [26]. We consider the first one of them, which can be written as:

$$\mathbf{L}_c = -k_1 \boldsymbol{\delta}\mathbf{q}_v - k_2 \boldsymbol{\omega}, \tag{29}$$

where $\mathbf{L}_c$ is the control torque, $\boldsymbol{\delta}\mathbf{q}_v = \boldsymbol{\delta}\mathbf{q}_{1:3}$, $\boldsymbol{\omega} = \boldsymbol{\omega}_{B/N}$, and k_1, k_2 are positive scalar gains. This is an attitude regulation controller, meaning that attitude is driven to a desired constant attitude $\mathbf{q}_d$, while driving $\boldsymbol{\omega}$ to $\boldsymbol{\omega}_d = 0$. The attitude error quaternion is defined by [24]

$$\boldsymbol{\delta}\mathbf{q} = \begin{bmatrix} \boldsymbol{\delta}\mathbf{q}_{1:3} \\ \delta q_4 \end{bmatrix} = \mathbf{q} \otimes \mathbf{q}_d^{-1} = \begin{bmatrix} \Xi^T(\mathbf{q}_d) \\ \mathbf{q}_d^T \end{bmatrix} \mathbf{q}, \tag{30}$$

where $\mathbf{q}$ is the current attitude, $\mathbf{q}_d$ is the desired attitude, $\otimes$ denotes quaternion product, and

$$\Xi(\mathbf{q}) = \begin{bmatrix} q_4\mathbf{I}_3 + [\mathbf{q}_{1:3}\times] \\ -\mathbf{q}_{1:3}^T \end{bmatrix}, \quad \mathbf{q} \equiv \begin{bmatrix} \mathbf{q}_{1:3} \\ q_4 \end{bmatrix}. \tag{31}$$

The quaternion product for two quaternions $\mathbf{q}$ and $\mathbf{p}$ is [24]

$$\mathbf{q} \otimes \mathbf{p} \equiv \begin{bmatrix} q_4\mathbf{I}_3 - [\mathbf{q}_{1:3}\times] & \mathbf{q}_{1:3} \\ -\mathbf{q}_{1:3}^T & q_4 \end{bmatrix} \mathbf{p}. \tag{32}$$

The error quaternion represents the rotation between the current attitude and goal attitude. The time derivative of the error quaternion is

$$\delta\dot{\mathbf{q}} = \dot{\mathbf{q}} \otimes \mathbf{q}_d^{-1}, \tag{33}$$

because $\mathbf{q}_d$ is constant. Then, using eq. (23) we can write

$$\delta\dot{\mathbf{q}} = \frac{1}{2}\Omega(\boldsymbol{\omega} - \boldsymbol{\omega}_d)\delta\mathbf{q} = \frac{1}{2}\Omega(\boldsymbol{\omega})\delta\mathbf{q}. \tag{34}$$

For a spacecraft with n reaction wheels, the net torque produced by the wheels on the spacecraft is

$$\mathbf{L}_c = -\mathbf{G}\mathbf{u}, \tag{35}$$

due to Newton's third law, where $\mathbf{u}$ is a vector of wheel torques. We can write the closed-loop dynamics of the spacecraft as

$$\mathbf{J}_c^B\dot{\boldsymbol{\omega}} = -k_1\delta\mathbf{q}_v - k_2\boldsymbol{\omega} - \boldsymbol{\omega} \times \left(\mathbf{J}_c^B\boldsymbol{\omega} + \mathbf{G}\mathbf{h}_a\right), \tag{36}$$

where we assume there is no net external torque ($\mathbf{L}_c^B = \mathbf{0}$).

Stability of the proposed control law is proven using Lyapunov's direct method. We define the following candidate Lyapunov function:

$$V(\delta\mathbf{q}, \boldsymbol{\omega}) = \frac{1}{2}\boldsymbol{\omega}^T\mathbf{J}_c^B\boldsymbol{\omega} + k_1\delta\mathbf{q}_v^T\delta\mathbf{q}_v + k_1(1 - \delta q_4)^2 \geq 0. \tag{37}$$

We can see that $V = 0$ when $\boldsymbol{\omega} = \mathbf{0}$ and $\delta\mathbf{q} = [0\ 0\ 0\ 1]^T$ which is the identity quaternion. This is the equilibrium point of the closed loop system.

The time derivative of V is

$$\dot{V} = \boldsymbol{\omega}^T\mathbf{J}_c^B\dot{\boldsymbol{\omega}} + 2k_1\delta\mathbf{q}_v^T\delta\dot{\mathbf{q}}_v - 2k_1(1 - \delta q_4)\delta\dot{q}_4. \tag{38}$$

Substituting eqs. (34) and (36) into eq. (38) yields

$$\dot{V} = -k_2\boldsymbol{\omega}^T\boldsymbol{\omega} \leq 0. \tag{39}$$

As $\dot{V}$ is not strictly negative, we must apply LaSalle's Invariance Principle to investigate whether there exist any trajectories which maintain $\dot{V}(t) = 0$ for a finite length of time. If $\dot{V}(t) = 0$ for a finite length of time, then from eq. (39) we know $\boldsymbol{\omega}(t) = \mathbf{0}$ and $\dot{\boldsymbol{\omega}}(t) = \mathbf{0}$. However, under these conditions eq. (36) shows the only solution is the trivial solution $\delta\mathbf{q}_v(t) = \mathbf{0}$. Because V is radially unbounded, we conclude the equilibrium point is globally asymptotically stable.

B. Torque Distribution Methods

The control law developed in section VII.A generates a 3×1 control torque vector $\mathbf{L}_c$. We generate this torque vector with the reaction wheels using $\mathbf{L}_c = -\mathbf{G}\mathbf{u}$, as stated in eq. (35). We now ask: given a specific $\mathbf{L}_c$, what $\mathbf{u}$ will satisfy the equality constraint eq. (35)? This is equivalent to asking: how should we *distribute* the torque requirement amongst the reaction wheels?

If $n = 3$ and $\text{Rank}(\mathbf{G}) = 3$, there is a unique solution for $\mathbf{u}$. For our spacecraft, $n = 3, N = 18 > 3$, so there are infinitely many solutions for $\mathbf{u}$ which satisfy eq. (35), as long as $\text{Rank}(\mathbf{G}) = 3$, i.e. $\mathbf{G}$ has full row rank. We can choose the optimal $\mathbf{u} = \mathbf{u}^*$ by minimizing some scalar cost function C while still meeting the constraint in eq. (35):

$$\begin{aligned} \min \quad & C(\mathbf{u}, \mathbf{q}, \boldsymbol{\omega}) \\ \text{subject to} \quad & -\mathbf{G}\mathbf{u} = \mathbf{L}_c \end{aligned} \tag{40}$$

Consider the quadratic cost function

$$C = \mathbf{u}^T \mathbf{Q}\mathbf{u}, \quad \mathbf{Q} > 0, \tag{41}$$

where $\mathbf{Q} \in \mathbb{R}^{n\times n}$ is a positive definite weighting matrix. To solve eqs. (40) and (41), we define the Hamiltonian $\mathcal{H} = \mathbf{u}^T \mathbf{Q}\mathbf{u} + \boldsymbol{\lambda}^T (\mathbf{G}\mathbf{u} + \mathbf{L}_c)$ and set $\frac{\partial \mathcal{H}}{\partial \mathbf{u}} = \mathbf{0}$. The solution to the optimization problem posed in eqs. (40) and (41) is

$$\mathbf{u}^* = -\mathbf{Q}^{-1}\mathbf{G}^T (\mathbf{G}\mathbf{Q}^{-1}\mathbf{G}^T)^{-1}\mathbf{L}_c, \tag{42}$$

where we assume $\text{Rank}(\mathbf{G}) = 3$. This torque distribution law minimizes the sum of the squares of the wheel torques, which is a proxy for total power exerted by all motors.

Another possible torque distribution cost function could be $C = \mathbf{h}_a^T \mathbf{h}_a$, where $\mathbf{h}_a$ is the vector of wheel momenta. Using this cost function would minimize the total reaction wheel momentum magnitude, which could also be a desirable feature.

VIII. Numerical Simulation

The numerical simulations of the proposed control law and torque distribution scheme for the tensegrity torus spacecraft are provided here. The goal is to test the performance of the control law under different operating conditions. The physical parameters used for the simulations are described in table 1. We chose a mid-range (approx. 1m) diameter and a lightweight chassis mass to represent a realistic application scenario. Typical values for reaction wheel size and mass were chosen to represent commercially available reaction wheels of this size class.

Table 1 Numerical Simulation Physical Parameters

N	=	number of T-Bar modules	6
n	=	number of reaction wheels	18
R_o	=	torus major radius	50 cm
ℓ	=	plate edge length	32 cm
$m_{chassis}$	=	total chassis mass	1 kg
m_{rw}	=	reaction wheel mass	200 g
r_{rw}	=	reaction wheel radius	6.3 cm
t_{rw}	=	reaction wheel thickness	2 cm
J_{si}	=	wheel moment of inertia in spin direction	3.969×10^{-4} kg m^2
J_{ti}	=	wheel moment of inertia transverse to spin dir.	2.051×10^{-4} kg m^2

We used a uniform toroidal mass distribution to simulate the inertia matrix of the chassis (spacecraft without reaction wheels), which has the following inertia matrix:

$$\mathbf{J}^B_{c,\text{no wheels}} = \begin{bmatrix} 0.1463 & 0 & 0 \\ 0 & 0.1463 & 0 \\ 0 & 0 & 0.2756 \end{bmatrix} \text{kg m}^2. \tag{43}$$

The inertia matrix $\mathbf{J}^B_c$ is computed with eq. (16):

$$\mathbf{J}^B_c = \begin{bmatrix} 0.5998 & 0 & 0 \\ 0 & 0.5998 & 0 \\ 0 & 0 & 1.1784 \end{bmatrix} \text{kg m}^2. \tag{44}$$

The numerical simulation was accomplished by using the MATLAB based `ode45` function to integrate the equations of motion to within a numerical tolerance of 1×10^{-6}.

A. Case 1: Attitude Maneuver with Zero Initial Angular Velocity

In the first scenario, the spacecraft has zero initial angular velocity. The initial attitude quaternion is random, and the desired attitude was selected as

$$\mathbf{q}(0) = [-0.7433,\ -0.5707,\ -0.0149,\ 0.3487]^T, \tag{45}$$

$$\mathbf{q}_d = [0,\ 0.7071,\ 0,\ 0.7071]^T. \tag{46}$$

The initial angular speeds of each reaction wheel was set to zero.

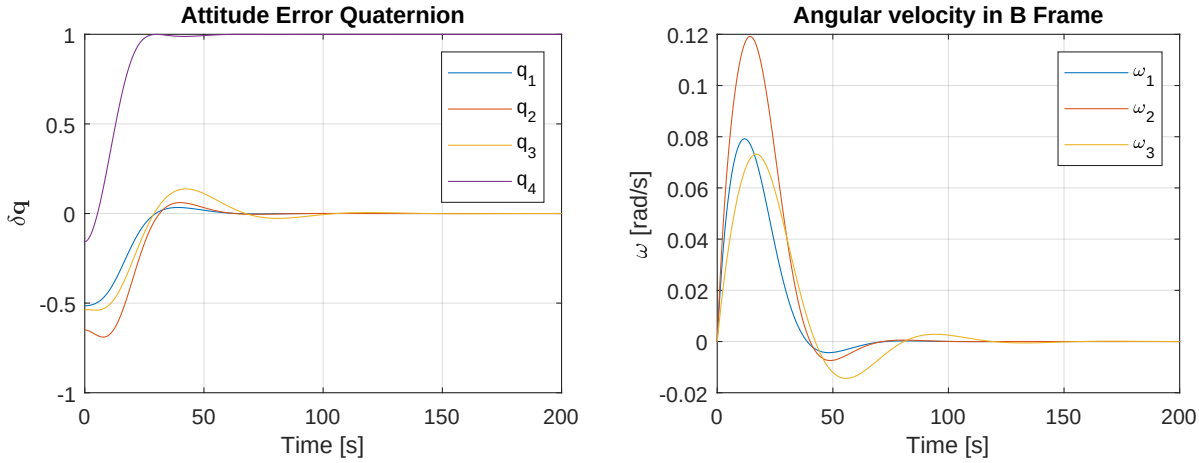

Fig. 3 Attitude error and angular velocity for zero initial angular velocity simulation.

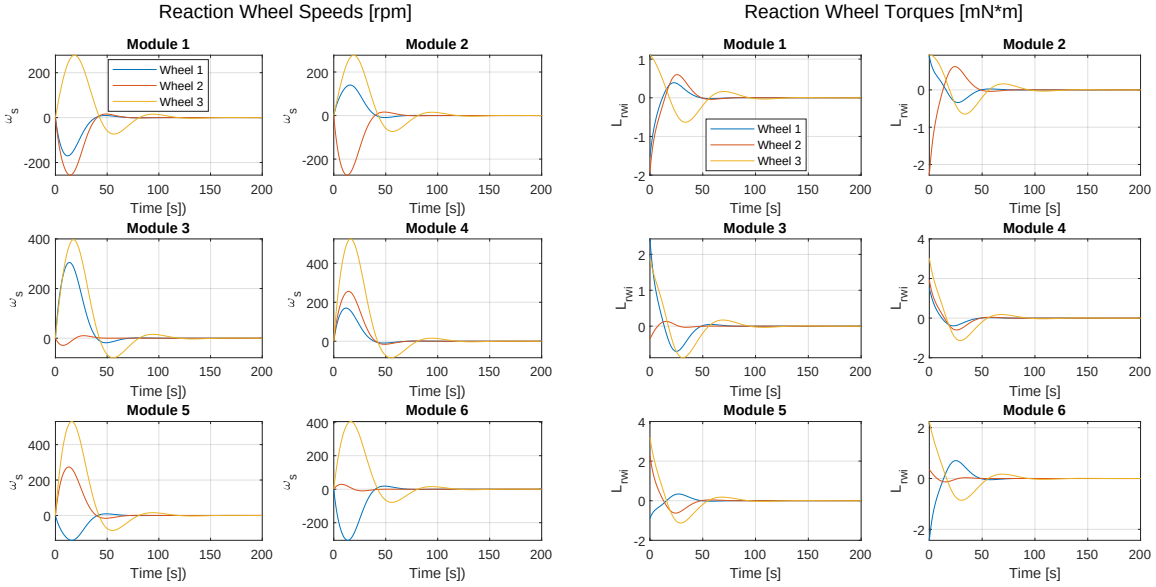

Fig. 4 Reaction wheel speeds and torques for zero initial angular velocity simulation.

The spacecraft must then navigate to the desired attitude. The positive control gains k_1 and k_2 were set to be

$$k_1 = 0.02, \quad k_2 = 0.1. \tag{47}$$

These gains were determined empirically by choosing increasingly smaller values until the commanded wheel torque

was within typical capabilities of small reaction wheels (< 10 mN m). The positive definite weight matrix $\mathbf{Q}$ was set to be $\mathbf{Q} = \mathbf{I}_n$, which is the $n \times n$ identity matrix.

The simulation results shown in figs. 3 and 4 show that the control law is able to successfully reorient the spacecraft within approximately 100s. We note that the reaction wheel speeds approach zero as $t \to \infty$. These results confirm that the proposed control law works as expected. The total kinetic energy of the system is given in fig. 5. Notice that the spacecraft has zero kinetic energy before and after the maneuver.

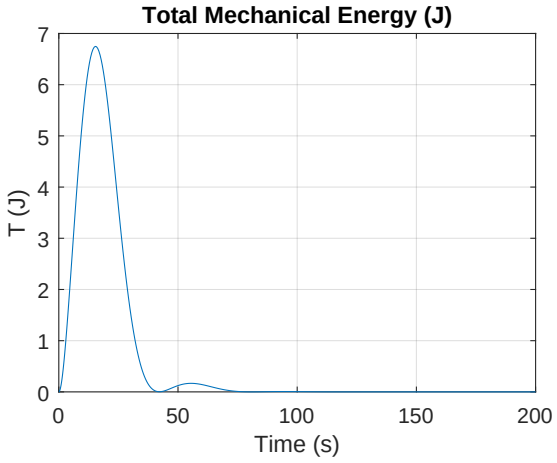

Fig. 5 Total energy for zero initial angular velocity simulation.

B. Case 2: Attitude Regulation with Non-Zero Initial Angular Velocity

In this case, $\boldsymbol{\omega}_{B/N}(0) \neq \mathbf{0}$. As a result, the reaction wheels must spin up to remove momentum from the rotating spacecraft. For this simulation, we set

$$\boldsymbol{\omega}_{B/N}(0) = [0.02,\ -0.04,\ 0.06]\text{rad/s}, \tag{48}$$

and we utilize the same initial and goal attitudes as the previous section.

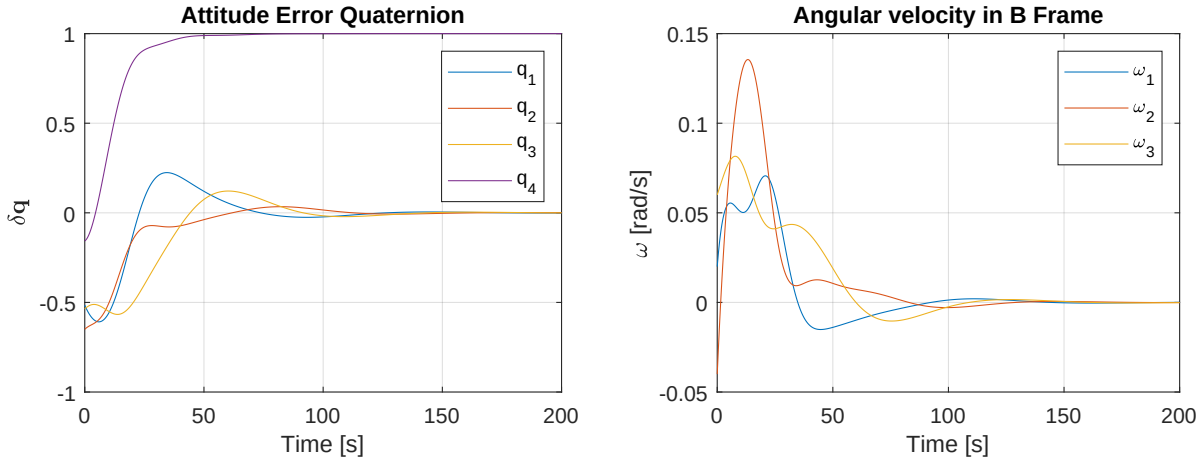

Fig. 6 Attitude error and angular velocity for non-zero initial angular velocity simulation.

The numerical results of this scenario are shown in figs. 6 and 7, which show that the control law is able to successfully reorient the spacecraft within approximately 150s. We note that the reaction wheel speeds do not approach zero as $t \to \infty$, but settle at a fixed value. This is because the spacecraft has no momentum-dumping capability, so the wheels must absorb the initial angular momentum which was present.

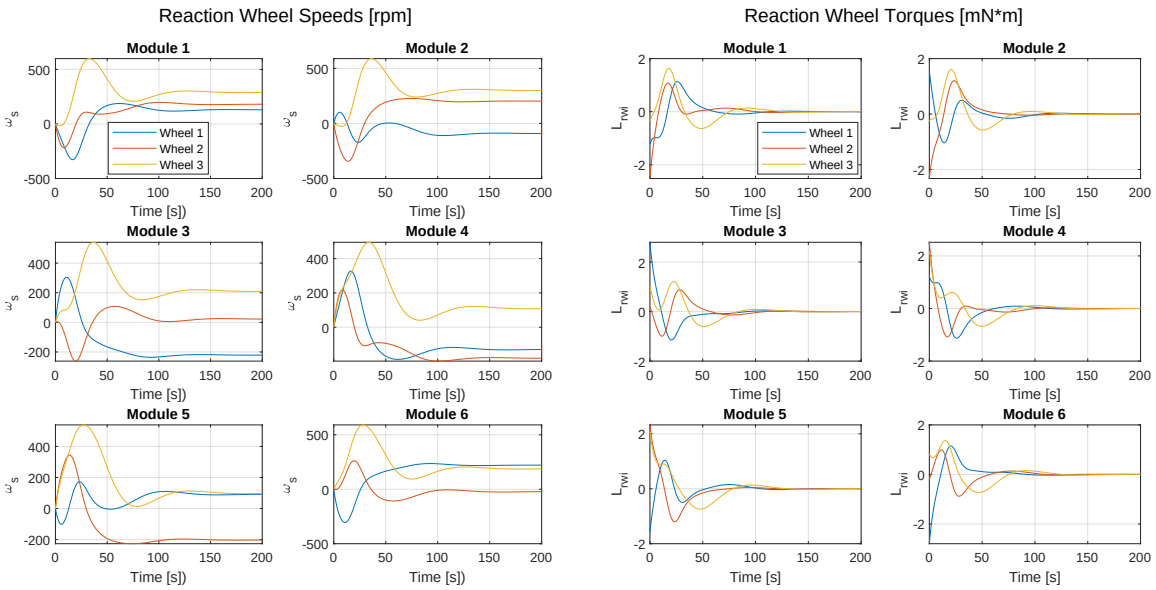

Fig. 7 Reaction wheel speeds and torques for non-zero initial angular velocity simulation.

IX. Conclusion

In this paper, a simple tensegrity-based structural module is proposed which can be duplicated and assembled into any number of reconfigurable lightweight space structures. The proposed module is shown to be equipped with 3-axis reaction wheels, which allow independent pointing and attitude control of each module within a larger spacecraft. Dynamics equations are developed for a tensegrity torus structure assembled out of the proposed modules, using a rigid-body simplification. A globally asymptotically stable feedback controller for attitude regulation is found for this structure and attitude maneuvers are simulated numerically. The proposed tensegrity gyroscopic structural module and the torus spacecraft composed of the modules have applications in in-space manufacturing and space habitats. The preliminary work presented in this paper forms a basis for optimism in realizing composable autonomous space systems from modular structural systems. Future work will investigate a wide variety of topologies for these applications.

References

[1] Fuller, R. B., "Tensile integrity structures," , 1959. US Patent 3.063.521.

[2] Snelson, K. D., "Continuous tension, discontinuous compression structures," 1965. US Patent 3,169,611.

[3] Skelton, R. E., and de Oliveira, M. C., *Tensegrity Systems*, Springer, 2009.

[4] Bel Hadj Ali, S. I., N., "Dynamic behavior and vibration control of a tensegrity structure," *International Journal of Solids and Structures*, Vol. 47, 2010, pp. 1285–1296.

[5] Masic, M., Skelton, R. E., and Gill, P. E., "Optimization of tensegrity structures," *International Journal of Solids and Structures*, Vol. 43, No. 16, 2006, pp. 4687–4703.

[6] Skelton, R. E., and de Oliveira, M. C., "Optimal complexity of deployable compressive structures," *Journal of the Franklin Institute*, Vol. 347, No. 1, 2010, pp. 228–256. https://doi.org/http://dx.doi.org/10.1016/j.jfranklin.2009.10.010.

[7] Goyal, R., and Skelton, R., "Tensegrity System Dynamics with Rigid Bars and Massive Strings," *Multibody System Dynamics*, Vol. 46(3), 2019, pp. 203–228. https://doi.org/10.1007/s11044-019-09666-4.

[8] Skelton, R. E., and de Oliveira, M. C., "Optimal tensegrity structures in bending: the discrete Michell truss," *Journal of the Franklin Institute*, Vol. 347, No. 1, 2010, pp. 257–283.

[9] Carpentieri, G., Skelton, R. E., and Fraternali, F., "Minimum mass and optimal complexity of planar tensegrity bridges," *International Journal of Space Structures*, Vol. 30, No. 3-4, 2015, pp. 221–243.

[10] Karnan, H., Goyal, R., Majji, M., Skelton, R. E., and Singla, P., "Visual feedback control of tensegrity robotic systems," *2017 IEEE/RSJ International Conference on Intelligent Robots and Systems (IROS)*, 2017, pp. 2048–2053. https://doi.org/10.1109/IROS.2017.8206022.

[11] Paul, C., Valero-Cuevas, F. J., and Lipson, H., "Design and control of tensegrity robots for locomotion," *IEEE Transactions on Robotics*, Vol. 22, No. 5, 2006, pp. 944–957. https://doi.org/10.1109/TRO.2006.878980.

[12] Adam, B., and Smith, I. F., "Active tensegrity: A control framework for an adaptive civil-engineering structure," *Computers & Structures*, Vol. 86, No. 23, 2008, pp. 2215 – 2223. https://doi.org/https://doi.org/10.1016/j.compstruc.2008.05.006.

[13] Sabelhaus, A. P., Bruce, J., Caluwaerts, K., Manovi, P., Firoozi, R. F., Dobi, S., Agogino, A. M., and SunSpiral, V., "System design and locomotion of SUPERball, an untethered tensegrity robot," *IEEE international conference on robotics and automation (ICRA)*, 2015, pp. 2867–2873.

[14] Tibert, A. G., and Pellegrino, S., "Deployable tensegrity mast," *In: 44th AIAA/ASME/ASCE/AHS/ASC, Structures, Structural Dynamics and Materials Conference and Exhibit, Norfolk , VA, USA.*, 2003, p. 1978. https://doi.org/10.2514/6.2003-1978.

[15] Murakami, H., "Static and dynamic analyses of tensegrity structures. Part 1. Nonlinear equations of motion," *International Journal of Solids and Structures*, Vol. 38(20), 2001, pp. 3599–3613.

[16] Goyal, R., Majji, M., and Skelton, R. E., "A Vector Approach for Analytical Dynamics of a System of Rigid Bars," *International Journal of Structural Stability and Dynamics*, Vol. 19, No. 08, 2019, p. 1950083. https://doi.org/10.1142/S0219455419500834.

[17] Goyal, R., Chen, M., Majji, M., and Skelton, R. E., "Gyroscopic Tensegrity Robots," *IEEE Robotics and Automation Letters*, Vol. 5, No. 2, 2020, pp. 1239–1246.

[18] Wie, B., *Space vehicle dynamics and control*, American Institute of Aeronautics and Astronautics, 2008.

[19] Vadali, S. R., and Oh, H.-S., "Space Station Attitude Control and Momentum Management: A Nonlinear Look," *Journal of Guidance, Control and Dynamics*, Vol. 15, No. 3, 1992.

[20] Hughes, P. C., *Spacecraft Attitude Dynamics*, Dover Publications, Mineola, NY, 2004.

[21] Gateway, "The Von Braun Rotating Space Station," *https://gatewayspaceport.com/von-braun-station/*, 2019.

[22] Goyal, R., Bryant, T., Majji, M., Skelton, R. E., and Longman, A., "Design and Control of Growth Adaptable Artificial Gravity Space Habitat," *AIAA SPACE and Astronautics Forum and Exposition*, 2017, p. 5141. https://doi.org/10.2514/6.2017-5141.

[23] Hogan, E. A., and Schaub, H., "Three-Axis Attitude Control Using Redundant Reaction Wheels with Continuous Momentum Dumping," *Journal of Guidance, Control, and Dynamics*, Vol. 38, No. 10, 2015, pp. 1865–1871. https://doi.org/10.2514/1.G000812, URL https://doi.org/10.2514/1.G000812.

[24] Markley, F. L., and Crassidis, J. L., *Fundamentals of Spacecraft Attitude Determination and Control*, Space Technology Library, Springer, New York, NY, 2014. https://doi.org/10.1007/978-1-4939-0802-8.

[25] Schaub, H., and Junkins, J. L., *Analytical Mechanics of Space Systems*, 3rd ed., AIAA Education Series, AIAA, Reston, VA, 2014.

[26] Wie, B., and Barba, P. M., "Quaternion feedback for spacecraft large angle maneuvers," *Journal of Guidance, Control, and Dynamics*, Vol. 8, No. 3, 1985, pp. 360–365. https://doi.org/10.2514/3.19988, URL https://doi.org/10.2514/3.19988.